



Fermi National Accelerator Laboratory

FERMILAB-Pub-93/392-E

E665

Production of Neutral Strange Particles in Muon-Nucleon Scattering at 490 GeV

The E665 Collaboration

*Fermi National Accelerator Laboratory
P.O. Box 500, Batavia, Illinois 60510*

December 1993

Submitted to *Zeitschrift fur Physik C*

Disclaimer

This report was prepared as an account of work sponsored by an agency of the United States Government. Neither the United States Government nor any agency thereof, nor any of their employees, makes any warranty, express or implied, or assumes any legal liability or responsibility for the accuracy, completeness, or usefulness of any information, apparatus, product, or process disclosed, or represents that its use would not infringe privately owned rights. Reference herein to any specific commercial product, process, or service by trade name, trademark, manufacturer, or otherwise, does not necessarily constitute or imply its endorsement, recommendation, or favoring by the United States Government or any agency thereof. The views and opinions of authors expressed herein do not necessarily state or reflect those of the United States Government or any agency thereof.

Production of Neutral Strange Particles in Muon-Nucleon Scattering at 490 GeV

THE FERMILAB E665 COLLABORATION

November 1993

Submitted to *Zeitschrift für Physik C*

Abstract

The production of K^0 , Λ and $\bar{\Lambda}$ -particles is studied in the E665 muon-nucleon experiment at Fermilab. The average multiplicities and squared transverse momenta are measured as a function of x_F and W^2 . Most features of the data can be well described by the Lund model. Within this model, the data on the K^0/π^\pm ratios and on the average K^0 multiplicity in the forward region favor a strangeness suppression factor s/u in the fragmentation process near 0.20. Clear evidence for QCD effects is seen in the average squared transverse momentum of K^0 and Λ particles.

M. R. Adams ⁽⁶⁾, M. Aderholz ⁽¹¹⁾, S. Aïd ^(9,a), P. L. Anthony ^(10,b), M. D. Baker ⁽¹⁰⁾, J. Bartlett ⁽⁴⁾, A. A. Bhatti ^(13,c), H. M. Braun ⁽¹⁴⁾, W. Busza ⁽¹⁰⁾, J. M. Conrad ⁽⁵⁾, G. Coutrakon ^(4,d), R. Davisson ⁽¹³⁾, I. Derado ⁽¹¹⁾, S. K. Dhawan ⁽¹⁵⁾, W. Dougherty ⁽¹³⁾, T. Dreyer ⁽¹⁾, K. Dziunikowska ⁽⁸⁾, V. Eckardt ⁽¹¹⁾, U. Ecker ^(14,e), M. Erdmann ^(1,e), A. Eskreys ⁽⁷⁾, J. Figiel ⁽⁷⁾, H. J. Gebauer ⁽¹¹⁾, D. F. Geesaman ⁽²⁾, R. Gilman ^(2,f), M. C. Green ^(2,g), J. Haas ⁽¹⁾, C. Halliwell ⁽⁶⁾, J. Hanlon ⁽⁴⁾, D. Hantke ⁽¹¹⁾, V. W. Hughes ⁽¹⁵⁾, H. E. Jackson ⁽²⁾, D. E. Jaffe ^(6,h), G. Jancso ⁽¹¹⁾, D. M. Jansen ^(13,i), K. Kadija ⁽¹¹⁾, S. Kaufman ⁽²⁾, R. D. Kennedy ⁽³⁾, T. Kirk ^(4,j), H. G. E. Kobrak ⁽³⁾, S. Krzywdzinski ⁽⁴⁾, S. Kunori ⁽⁹⁾, J. J. Lord ⁽¹³⁾, H. J. Lubatti ⁽¹³⁾, D. McLeod ⁽⁶⁾, S. Magill ^(6,j), P. Malecki ⁽⁷⁾, A. Manz ⁽¹¹⁾, H. Melanson ⁽⁴⁾, D. G. Michael ^(5,k), W. Mohr ⁽¹⁾, H. E. Montgomery ⁽⁴⁾, J. G. Morfin ⁽⁴⁾, R. B. Nickerson ^(5,l), S. O'Day ^(9,m), K. Olkiewicz ⁽⁷⁾, L. Osborne ⁽¹⁰⁾, V. Papavassiliou ^(15,j), B. Pawlik ⁽⁷⁾, F. M. Pipkin ^(5,n), E. J. Ramberg ^(9,m), A. Röser ^(14,o), J. J. Ryan ⁽¹⁰⁾, C. W. Salgado ⁽⁴⁾, A. Salvarani ^(3,p), H. Schellman ⁽¹²⁾, M. Schmitt ^(5,q), N. Schmitz ⁽¹¹⁾, K. P. Schuler ^(15,r), H. J. Seyerlein ⁽¹¹⁾, A. Skuja ⁽⁹⁾, G. A. Snow ⁽⁹⁾, S. Söldner-Rembold ^(11,s), P. H. Steinberg ⁽⁹⁾, H. E. Stier ⁽¹⁾, P. Stopa ⁽⁷⁾, R. A. Swanson ⁽³⁾, R. Talaga ^(9,j), S. Tentindo-Repond ^(2,t), H.-J. Trost ^(2,u), H. Venkataramania ⁽¹⁵⁾, M. Wilhelm ⁽¹⁾, J. Wilkes ⁽¹³⁾, Richard Wilson ⁽⁵⁾, W. Wittek ⁽¹¹⁾, S. A. Wolbers ⁽⁴⁾, T. Zhao ⁽¹³⁾

(The Fermilab E665 Collaboration)

- ⁽¹⁾ *Albert-Ludwigs-Universität Freiburg i. Br., Germany*
- ⁽²⁾ *Argonne National Laboratory, Argonne IL USA*
- ⁽³⁾ *University of California, San Diego, CA USA*
- ⁽⁴⁾ *Fermi National Accelerator Laboratory, Batavia, IL USA*
- ⁽⁵⁾ *Harvard University, Cambridge, MA USA*
- ⁽⁶⁾ *University of Illinois, Chicago, IL USA*
- ⁽⁷⁾ *Institute for Nuclear Physics, Krakow, Poland*
- ⁽⁸⁾ *Institute for Nuclear Physics, Academy of Mining and Metallurgy, Krakow, Poland*
- ⁽⁹⁾ *University of Maryland, College Park, MD USA*
- ⁽¹⁰⁾ *Massachusetts Institute of Technology, Cambridge, MA USA*
- ⁽¹¹⁾ *Max-Planck-Institut für Physik, Munich, Germany*
- ⁽¹²⁾ *Northwestern University, Evanston, IL USA*
- ⁽¹³⁾ *University of Washington, Seattle, WA USA*
- ⁽¹⁴⁾ *University of Wuppertal, Wuppertal, Germany*
- ⁽¹⁵⁾ *Yale University, New Haven, CT USA*

- ^a Current address: Alaskaweg 20, 22145 Hamburg, Germany.
- ^b Current address: Lawrence Livermore National Laboratory, Livermore CA 94550, USA.
- ^c Current address: The Rockefeller University, New York NY 10021, USA.
- ^d Current address: Loma Linda University Medical Center, Loma Linda CA 92350, USA.
- ^e Current address: Universität Heidelberg, 69120 Heidelberg, Germany.
- ^f Current address: Rutgers University, Piscataway, NJ 08855, USA.
- ^g Current address: LeCroy Research Systems, Spring Valley, NY 10977, USA.
- ^h Current address: Laboratoire de l'Accélérateur Linéaire, F-91405 Orsay, France.
- ⁱ Current address: Los Alamos National Laboratory, Los Alamos, NM 87545, USA.
- ^j Current address: Argonne National Laboratory, Argonne, IL 60439, USA.
- ^k Current address: California Institute of Technology, Pasadena, CA 91125, USA.
- ^l Current address: Oxford University, Oxford OX1 3RH, UK.
- ^m Current address: Fermi National Accelerator Laboratory, Batavia, IL 60510, USA.
- ⁿ Deceased
- ^o Current address: Universität Bochum, 44801 Bochum, Germany.
- ^p Current address: A.T. & T., Bell Labs, 2000 North Naperville Road, Naperville, IL USA.
- ^q Current address: University of Wisconsin, Madison, WI 53706, USA.
- ^r Current address: Superconducting Super Collider Laboratory, Dallas, TX 75237, USA.
- ^s Current address: Albert-Ludwigs-Universität Freiburg, 79104 Freiburg, Germany.
- ^t Current address: Northern Illinois University, Dekalb, IL 60115, USA.
- ^u Current address: Texas A&M University, College Station, Texas 77843-4242

1 Introduction

This paper presents an analysis of neutral-strange-particle production (K^0 , Λ , $\bar{\Lambda}$) in muon-nucleon interactions at 490 GeV. It extends previous measurements in lepton-nucleon experiments [1]-[6] to higher values of the hadronic mass W , up to 30 GeV.

Due to their strange-quark content, strange particles provide information on the $s(\bar{s})$ quarks in the nucleon, the $s(\bar{s})$ and $c(\bar{c})$ quark production in the photon-gluon fusion reaction, and on the production of strange quarks in the fragmentation process. Previous measurements have shown that neutral-strange-particle production in lepton-nucleon scattering can be successfully described in the framework of the quark-parton model (QPM). In the present experiment, because of the extended W range, it becomes possible to also identify some of the additional effects expected from Quantum-Chromodynamics (QCD).

The deep-inelastic muon-nucleon scattering process can be described by the exchange of a single virtual photon. In the following the target nucleon is assumed to be at rest in the laboratory frame. The kinematic variables of the event are then defined by

$$\begin{aligned}
 Q^2 &= -2m_\mu^2 + 2E_\mu E'_\mu - 2p_\mu p'_\mu \cos \Theta && \text{negative square of the virtual} \\
 &&& \text{photon four-momentum,} \\
 W^2 &= -Q^2 + 2M\nu + M^2 && \text{squared invariant mass of} \\
 &&& \text{the hadronic system,} \\
 x_{Bj} &= \frac{Q^2}{2M\nu} && \text{Bjorken-}x, \\
 \nu &= E_\mu - E'_\mu && \text{leptonic energy transfer} \\
 &&& \text{in the laboratory frame,}
 \end{aligned} \tag{1}$$

where m_μ is the muon mass, E_μ (E'_μ) is the laboratory energy and p_μ (p'_μ) the laboratory momentum of the incident (scattered) muon, Θ is the muon scattering angle in the laboratory frame and M is the nucleon mass.

The hadronic center-of-mass system (cms) is defined as the system formed by the virtual photon and the target nucleon. The hadron variables used are Feynman- x , $x_F = 2p_L^*/W$, and the transverse momentum p_T , where p_L^* and p_T are the longitudinal and transverse momentum (relative to the direction of the virtual photon) of the hadron in the cms. The forward and backward hemispheres are defined by $x_F > 0$ and $x_F < 0$, respectively.

2 Experimental procedure

The data were obtained in the 1987/88 fixed target run of the E665 experiment at Fermilab. Positive muons with an average energy of 490 GeV were scattered off a liquid hydrogen or deuterium target. Charged secondary particles were reconstructed

and measured in an open geometry forward spectrometer (FS), comprising two magnets of opposite polarity and several sets of multiwire proportional chambers. Muons were detected and identified by four sets of scintillation and proportional chambers behind a hadron absorber. Photons were reconstructed in an electromagnetic calorimeter, which was placed upstream of the hadron absorber. For part of the data, photographic information from a streamer chamber (SC) was also available. The SC was located inside the first magnet and surrounded the target.

Details about the detector and the triggers can be found in [7]. Comprehensive descriptions of the processing of the FS and SC data are given in [8, 9] and [10, 11] respectively.

2.1 Monte Carlo simulation of the experiment and Monte Carlo predictions

In order to determine the corrections to the data (see Sect. 2.4) the experiment was simulated in detail by a Monte Carlo (MC) program. The Lund programs LEPTO 4.3 and JETSET 4.3 [12] served as the physics generators, while the detector was simulated using the GEANT program package [13]. Particle decays, secondary interactions and a detailed simulation of the detector were included. The MC generated events were subjected to the identical analysis as the data. For further details about the MC simulation see [10, 11].

In Sect. 3, the corrected experimental data are compared with predictions of the Lund model. For this comparison the program versions LEPTO 6.1 [14], JETSET 7.3 [15] were used, which contain QCD corrections in the form of matrix elements. The parameters of the model were set to their default values, except for the strangeness suppression factor s/u (PARJ (2)), which was set to 0.20 (see subsection 3.4). The values of some parameters in JETSET 7.3, which are relevant for the present analysis, are compiled in Table 1. The parton distributions EHLQ set 1 from ref. [16] were used, in which the ratio of \bar{s} quarks to \bar{u} and \bar{d} quarks in the proton ($2\bar{s}/(\bar{u} + \bar{d})$) is equal to 0.43 at $Q^2 = 5 \text{ GeV}^2$.

2.2 Selection of events

In the present analysis [17] only data obtained with the ‘Large Angle Trigger’ are used. This trigger accepted essentially only muon scattering angles above 3 mrad. For streamer chamber pictures to be taken at least two hits (outside the beam region) were required in the non-bending planes of the PCN detector, in order to enhance the fraction of events in the streamer chamber pictures which had a hadron. The PCN chamber is a proportional chamber in the field free region between the two magnets.

In this analysis only events which fulfill the following conditions are included:

$$\begin{aligned}
 \Theta &> 3.5 \text{ mrad} \\
 Q^2 &> 1 \text{ GeV}^2 \\
 x_{Bj} &> 0.003
 \end{aligned}
 \tag{2}$$

$$0.1 < \nu/E_\mu < 0.85.$$

The cuts in Θ and Q^2 sharpen somewhat the cuts implied by the trigger condition. The cut in x_{Bj} removes events which are due to elastic μe scattering, while the upper limit in ν/E_μ excludes the kinematic region where radiative effects are large. By the lower limit in ν/E_μ the region of poor resolution in ν is excluded.

In the event sample defined by (2) residual contamination by radiative events is removed using the information from the electromagnetic calorimeter. An event is excluded if the number of energy clusters in the calorimeter is ≤ 2 and if, in addition, the total energy deposited in the calorimeter exceeds 0.5ν .

After all cuts the total number of H_2 and D_2 events amounts to 18600 and 71000 respectively, with average values of 17.1 GeV for W , 8.6 GeV² for Q^2 , 185 GeV for ν and 0.036 for x_{Bj} . The fraction of events with SC information is 24% for the H_2 and 15% for the D_2 sample.

The acceptance of the FS is essentially restricted to the forward cms hemisphere (with a tail extending down to $x_F \approx -0.2$), while the SC data cover the whole x_F region. For the results to be presented on the backward (forward) region only the events with SC (FS) information are used. It has been checked that the SC and FS data sets give consistent results in the x_F region which is covered by both the SC and the FS.

To increase the statistical significance, the H_2 and D_2 data have been combined for this analysis.

2.3 Selection of neutral strange particles

Neutral strange particles (V^0 particles) are detected via their decays into charged particles:

$$K^0 \rightarrow \pi^+\pi^-, \Lambda \rightarrow p\pi^-, \bar{\Lambda} \rightarrow \bar{p}\pi^+ . \quad (3)$$

In the following no distinction is made between K^0 and \bar{K}^0 and both are denoted by K^0 . Decay vertices of possible V^0 candidates are found in the experiment by combining oppositely charged particles, which were not both associated to the primary interaction vertex, and determining the point of closest approach for the two particle trajectories (geometric decay vertex fit). For decay vertices with acceptable vertex fit probability (> 0.001) kinematic fits* are performed for the decay hypotheses (3) and for the hypothesis of a photon conversion: $\gamma \rightarrow e^+e^-$. In these (3-constraint) fits the neutral particles are assumed to point to the primary vertex, i.e. the direction of flight of the V^0 particle is taken to be given by the distance vector between the primary and the decay vertex.

If the χ^2 -probability of the kinematic fit is acceptable (> 0.01) for both the Λ and the $\bar{\Lambda}$ hypothesis, the ambiguity is resolved by assigning the proton (or antiproton) mass to the decay track with the higher momentum (for Λ hyperons with a momentum greater than 300 MeV/c the proton momentum is always greater than the pion

*The kinematic fits are performed using the SQUAW fit program [18].

momentum). All further criteria for selecting K^0 , Λ and $\bar{\Lambda}$ candidates are summarized in Table 2a and 2b for the FS and SC data sets respectively.

The final sample of neutral strange particles consists of 1266 K^0 , 123 Λ and 116 $\bar{\Lambda}$ candidates in the FS data set. In the SC data set the number of accepted V^0 particles is 308 K^0 and 88 Λ , of which 116 K^0 and 58 Λ are formed by particle tracks seen in the SC only (see Table 3). Only the latter ones are used in the analysis of the strange particles in the backward region ($-1 < x_F < 0$).

The V^0 selection criteria are the result of extensive Monte Carlo studies (see Sect. 2.1). The Monte Carlo simulation was able to accurately reproduce many aspects of the data. Also the reduction rates for the number of V^0 candidates in the different steps of the analysis were found to be very similar in the data and in the Monte Carlo. This indicates that background processes are also modeled properly.

For the FS data set (Table 3), the fraction of wrong candidates, as determined by the Monte Carlo calculations, in the final sample of K^0 candidates is 10.4%, with 5.9% being due to wrongly interpreted Λ or $\bar{\Lambda}$ and 4.5% either due to K^0 from secondary interactions or due to pairs of oppositely charged particles, which do not originate from K^0 decays but which are kinematically consistent with the decay of a K^0 pointing to the primary interaction vertex. The corresponding background in the Λ sample amounts to 16.4%, with 6.6% and 3.8% being due to wrongly interpreted K^0 and γ respectively. The amount of background in the final $\bar{\Lambda}$ sample is about 2/3 of that in the final Λ sample. One reason for the reduced background is the fact that in secondary interactions $\bar{\Lambda}$ production is strongly suppressed as compared to Λ production. The contribution to the background from $\bar{\Lambda}$ produced in a secondary interaction is therefore reduced.

The amount of background in the SC data set (Table 3) is significantly larger than in the FS data set, and it is mainly due to pairs of oppositely charged particles, being kinematically consistent with a V^0 pointing to the primary vertex. The larger background in the SC as compared to the FS data set has several reasons: the geometrical resolution (position error of a track perpendicular to its direction) of the SC is worse by a factor of 8 than that of the FS, making the cuts on the geometric-fit and the kinematic-fit probabilities less effective; the larger average multiplicity of SC tracks leads to a larger background due to pairs of tracks which by accident are kinematically consistent with a V^0 decay pointing to the primary interaction vertex. Because of the large background contributions, $\bar{\Lambda}$ production is not studied in the SC data set.

The distributions of the effective ($\pi^+\pi^-$) and ($p\pi^-$) mass for the final samples, before applying the effective mass cuts, of K^0 and Λ candidates in the FS data set are shown in Fig. 1. The contribution from tracks with very different measurement errors on the track parameters (due to different track lengths) explains the particular shape of the mass distribution for K^0 , which can be well approximated by a superposition of two Gaussians on top of a flat background. The mass resolution as determined from the widths of the Gaussians fitted to the data is 6 to 21 MeV for K^0 and 4 MeV for Λ .

2.4 Correction of the data

The number of V^0 candidates is corrected in two steps. In the first step the number of fake V^0 is subtracted, which is assumed to be proportional to the number of reconstructed events:

$$M_{\text{data}}^{\text{rec},V^0} = M_{\text{data}}^{\text{rec}} - \beta_{\text{MC}} \cdot N_{\text{data}}^{\text{rec}}.$$

In this expression $M_{\text{data}}^{\text{rec}}$ is the number of V^0 candidates, $N_{\text{data}}^{\text{rec}}$ the number of reconstructed events and $M_{\text{data}}^{\text{rec},V^0}$ the estimated number of correctly reconstructed V^0 particles in the data. β_{MC} is the number of fake V^0 per reconstructed event as determined in the MC sample

$$\beta_{\text{MC}} = \frac{M_{\text{MC}}^{\text{rec, fake}}}{N_{\text{MC}}^{\text{rec}}}.$$

The correction from $M_{\text{data}}^{\text{rec},V^0}$ to the total number of produced V^0 ($M_{\text{data}}^{\text{corr}}$) in the data is performed by applying a multiplicative correction factor obtained from the MC sample

$$M_{\text{data}}^{\text{corr}} = \left(\frac{M_{\text{MC}}^{\text{gen}}}{M_{\text{MC}}^{\text{rec},V^0}} \right) \cdot M_{\text{data}}^{\text{rec},V^0}.$$

Here $M_{\text{MC}}^{\text{gen}}$ is the total number of produced V^0 and $M_{\text{MC}}^{\text{rec},V^0}$ the number of correctly reconstructed V^0 in the MC sample. In a similar manner the number of reconstructed events ($N_{\text{data}}^{\text{rec}}$) is corrected. The corrected number of events is determined as

$$N_{\text{data}}^{\text{corr}} = \left(\frac{N_{\text{MC}}^{\text{gen}}}{N_{\text{MC}}^{\text{rec}}} \right) \cdot N_{\text{data}}^{\text{rec}},$$

where $N_{\text{MC}}^{\text{gen}}$ is the number of generated events and $N_{\text{MC}}^{\text{rec}}$ the number of reconstructed events in the MC sample. The average corrected V^0 multiplicities are then determined by

$$\langle n \rangle = \frac{M_{\text{data}}^{\text{corr}}}{N_{\text{data}}^{\text{corr}}}.$$

The corrections account for effects due to the geometric acceptance of the detector, trigger inefficiencies, inefficiencies in the track and vertex reconstruction, secondary interactions, decays and photon conversions, for smearing of the kinematic quantities due to measurement errors and radiative effects, for the background of fake V^0 in the sample of V^0 candidates, for the selections of V^0 candidates and for unobserved (including neutral) decays of K^0 , Λ and $\bar{\Lambda}$. The errors quoted in the text and in the tables and drawn in the figures include only the statistical error of the data and the statistical error of the correction.

Systematic errors were estimated by comparing the results obtained with different versions of the Monte Carlo program and using different selection criteria for the V^0 candidates. With the binnings of the kinematic variables chosen in this analysis the systematic and statistical errors of the average V^0 multiplicities are of comparable size.

3 Results

All results to be presented in this section have been corrected. Some of them will be compared with MC predictions using the Lund model (see Sect. 2.1). The Monte Carlo events may be classified according to:

- A - no QCD corrections (QPM)
- B - gluon radiation
- C - photon-gluon fusion.

The latter two processes, gluon radiation and photon-gluon fusion, are expected from perturbative QCD. The relative size of the various samples and the average multiplicities of K^0 , Λ and $\bar{\Lambda}$ particles in each of the samples are listed in Table 4. Neutral strange particle production appears to be enhanced in the QCD samples B and C and K^0 production is particularly strong in the photon-gluon fusion sample C.

In the figures the curves referred to as ‘no QCD’ are obtained by considering only the events of class A, those referred to as ‘with QCD’ by considering the events of all three classes A, B and C.

3.1 x_F distributions

The normalized distributions of x_F for K^0 , Λ and $\bar{\Lambda}$ are shown in Fig. 2 and listed in Table 5. The x_F distribution for K^0 has a maximum around $x_F \approx 0$ and decreases approximately exponentially with increasing $|x_F|$, with a steeper drop in the backward than in the forward region. By fitting the expression $a \exp(-bx_F)$ to the K^0 data in the forward region, b is found to be 6.85 ± 0.24 (Table 6). The forward-backward asymmetry, defined as $(F - B)/(F + B)$, where F and B are the number of particles travelling in the forward and backward cms hemispheres respectively, is measured as 0.19 ± 0.14 (see Table 7).

The bulk of the Λ -particles are produced in the backward region, where the Λ -multiplicity depends only weakly on x_F . In the forward region it decreases approximately exponentially, with a slope parameter of $b = 5.94 \pm 1.03$. The forward-backward asymmetry is determined as -0.44 ± 0.14 .

For reasons of limited statistics and because of large background contributions, $\bar{\Lambda}$ production was only measured in the forward region, from the FS data alone. In this kinematic range Λ and $\bar{\Lambda}$ production are very similar, with respect to both size and shape of the x_F distribution. The integrated average forward multiplicity is 0.022 ± 0.004 for Λ and 0.020 ± 0.003 for $\bar{\Lambda}$ (Table 7). The slope parameter b for $\bar{\Lambda}$ is 6.50 ± 0.83 . For the comparison of Λ and $\bar{\Lambda}$ production in the forward region see also Sect. 3.5. In the analysis of ref. [1], where both Λ and $\bar{\Lambda}$ were measured in the whole x_F region, $\bar{\Lambda}$ production was found to be strongly suppressed relative to Λ production in the backward region.

As can be seen from Table 6, the slope of the x_F distribution in the forward region is similar for K^0 , Λ and $\bar{\Lambda}$ particles. The slope for K^0 mesons is also comparable to that measured for charged hadrons in the same experiment [19].

The curves drawn in Fig. 2 are the predictions of the Lund model including (solid lines) and not including QCD corrections (dashed lines). The two predictions, which mainly reflect the behavior due to the QPM, are qualitatively very similar and describe the data fairly well.

3.2 Dependence of average multiplicities on x_{Bj} , Q^2 , and W^2

The average forward multiplicities $\langle n_F \rangle$ of K^0 , Λ and $\bar{\Lambda}$ are shown as a function of x_{Bj} , Q^2 and W^2 in Fig. 3. While there is no clear dependence on x_{Bj} or Q^2 , $\langle n_F \rangle$ increases with increasing W^2 , for all three particle types. Fits of the expression $a + b \cdot \ln(W^2/\text{GeV}^2)$ to the data points yield the parameter values listed in Table 8. From Fig. 4 one can see that the multiplicity increase for K^0 mesons in the forward region is restricted to the region $x_F < 0.3$. Above $x_F \approx 0.3$ the average K^0 multiplicity is independent of W^2 (see also Table 9). It should be mentioned that the average W in the different Q^2 bins of Fig. 3 are very similar, so that no reflection of the W dependence of $\langle n_F \rangle$ is expected in the plot of $\langle n_F \rangle$ versus Q^2 .

The average forward multiplicity of K^0 mesons from this experiment is compared with data from an (anti-)neutrino proton experiment [6] in Fig. 5. Although the results from the two experiments appear to be consistent as far as the W dependence is concerned, one has to keep in mind that the relative contributions from different flavors of the struck quark are different in the various reactions, due to the different couplings of γ , W^+ and W^- to the quarks and due to the different x_{Bj} ranges covered in the different reactions.

In Figs. 6 and 7 the average total multiplicity of K^0 and Λ particles is plotted as a function of W^2 and compared with corresponding results from a μp [4], a $\nu(\bar{\nu})p$ [6], a νNe [3] and an $\bar{\nu}\text{Ne}$ [5] experiment. The new data in the high W region from this experiment are consistent with an increase of $\langle n(K^0) \rangle$ with W^2 and the weak dependence of $\langle n(\Lambda) \rangle$ on W^2 , as observed in the μ and ν , $\bar{\nu}$ experiments.

The numerical values of the average K^0 , Λ and $\bar{\Lambda}$ multiplicities as a function of W^2 , for different regions of x_F , are listed in Tables 10 and 11 respectively.

3.3 p_T^2 distributions

The transverse momentum p_T of hadrons in lepton-nucleon scattering is mainly due to the following sources

- quark and gluon fragmentation
- primordial transverse momentum of the partons in the nucleon
- QCD processes (gluon emission and photon-gluon fusion).

It is known that p_T is particularly sensitive to QCD processes [20, 21].

The p_T^2 -distributions were investigated separately in the forward and backward regions, for K^0 mesons also separately in three intervals of x_F in the forward region. In all cases the data are consistent with an exponential decrease of the form $\alpha \exp(-\beta p_T^2)$ (see Table 12 and Fig. 8).

The dependence of the average p_T^2 on x_F is shown in Fig. 9. For K^0 mesons there is a significant rise of $\langle p_T^2 \rangle$ with increasing x_F in the forward region, a behavior which is also clearly seen in Fig. 8 as a widening of the p_T^2 distribution. For Λ hyperons one observes clearly higher $\langle p_T^2 \rangle$ in the forward than in the backward region and, in the forward region, Λ and $\bar{\Lambda}$ data agree within the errors.

All this behavior is qualitatively reproduced by the Lund model, when QCD processes are included (solid lines). Without QCD processes (dashed lines) the model predicts a very weak dependence on x_F and no forward-backward asymmetry of $\langle p_T^2 \rangle$.

In Fig. 9 $\langle p_T^2 \rangle$ is also drawn for the subsamples A+B (dashed-dotted lines) and A+C (dotted lines) of Monte Carlo events. Of the two QCD processes gluon emission and photon-gluon fusion, clearly the latter gives the dominant contribution to $\langle p_T^2 \rangle$ in the forward region.

In Fig. 10 $\langle p_T^2 \rangle$ for K^0 , Λ and $\bar{\Lambda}$ particles is displayed as a function of W^2 , separately for the forward and backward region. Fig. 11 shows $\langle p_T^2 \rangle$ for K^0 mesons as a function of W^2 , in three x_F bins of the forward region. While for the whole forward or for the whole backward region (Fig. 10) the data for K^0 , Λ and $\bar{\Lambda}$ show only little or no dependence on W^2 , one can see an increase of $\langle p_T^2 \rangle$ with increasing W^2 for K^0 mesons with $x_F > 0.1$ (Fig. 11). This is qualitatively consistent with the Lund model in which the contribution to $\langle p_T^2 \rangle$ from QCD processes is increasing with increasing W^2 and x_F . The values of $\langle p_T^2 \rangle$ for K^0 mesons and their variation with W^2 and x_F are very similar to the corresponding results obtained for charged hadrons in the same experiment [19].

The behavior of $\langle p_T^2 \rangle$ of K^0 mesons as a function of Q^2 , in three bins of x_F in the forward region, is shown in Fig. 12. For the experimental data the variation with Q^2 is qualitatively similar to that with W^2 . This is in contrast to the theoretical prediction (including QCD corrections, solid lines in Fig. 12), which at high x_F suggests a rise of $\langle p_T^2 \rangle$ with W^2 and nearly no dependence on Q^2 . It is interesting to note that in an analysis of charged hadrons in the same experiment [22] $\langle p_T^2 \rangle$ was also found to increase with Q^2 , in contrast to the Monte Carlo prediction.

3.4 K^0/π ratio and strange quark suppression

The K^0/π^\pm ratios were determined from the experimental K^0/hadron^\pm ratios by applying appropriate correction factors as determined by Monte Carlo. The corrected K^0/π ratios are displayed in Fig. 13 as a function of x_F and, for the forward region, as a function of W^2 . Both the K^0/π^+ and the K^0/π^- ratios rise with increasing x_F . The pions are to a larger extent than the K^0 mesons decay products of resonances, which explains the rather low K^0/π^\pm ratios at low x_F . At large x_F ($x_F \gtrsim 0.3$) the K^0/π^+ ratio approaches a smaller value (≈ 0.3) than the K^0/π^- ratio (≈ 0.4), since in this

x_F range the π^+ multiplicity is greater than the π^- multiplicity. The latter fact is due to the stronger coupling of the photon to u -valence than to d -valence quarks.

There is no indication of a W dependence of the ratio of average forward K^0 and π multiplicities, and the value of the ratio is ≈ 0.16 (see Fig. 13).

The curves drawn in Fig. 13 (and Fig. 14) represent the predictions of the Lund Monte Carlo program (including QCD corrections) for two values of the strangeness suppression factor s/u : 0.20 (solid lines) and 0.30 (dashed-dotted lines). The data on the K^0/π^\pm ratios (Fig. 13) and on the average forward K^0 multiplicity (Fig. 14) clearly favor the lower s/u value. Other experiments, using different methods and/or different models for extracting s/u , find s/u values between 0.1 and 0.6 [23–32, 4]. The default value for this parameter in the JETSET 7.3 program is 0.30 (see also Table 1).

3.5 Comparison of Λ and $\bar{\Lambda}$ production

The ratio of the average Λ and $\bar{\Lambda}$ multiplicities is displayed in Fig. 15 as a function of x_F , p_T^2 and W^2 for the forward region. The ratio is consistent with 1 everywhere, but also with the expectation from the Lund model. In this model the Λ and $\bar{\Lambda}$ multiplicities are predicted to be very similar, with some variation of their ratio with x_F . Due to the presence of valence quarks, Λ production is slightly favored over $\bar{\Lambda}$ production at larger x_F .

4 Summary

In this analysis the production of K^0 , Λ and $\bar{\Lambda}$ particles in muon-nucleon interactions is studied at hadronic masses W between 10 and 30 GeV.

The analysis confirms the main features of neutral-strange-particle production, which have been observed previously at lower hadronic masses :

- an approximate logarithmic rise with W^2 of the average forward multiplicities,
- K^0 production which is slightly favored in the forward region, Λ production which is predominantly backward,
- similarity of forward Λ and $\bar{\Lambda}$ production.

These are features which are expected in the QPM. Clear evidence is seen for QCD effects in the average squared transverse momentum of K^0 and Λ particles :

- clearly higher $\langle p_T^2 \rangle$ in the forward than in the backward hemisphere, for both K^0 and Λ particles,
- a rise of $\langle p_T^2 \rangle$ with x_F and W^2 for K^0 mesons in the forward region.

When compared with Lund model predictions, the experimental data on the average forward multiplicity of K^0 mesons and on the K^0/π^\pm ratios clearly favor a strangeness-suppression factor s/u close to 0.20.

Acknowledgements

We wish to thank all those persons, both at Fermilab and the participating institutions, who have contributed to the success of this experiment. We thank B. Leupold, P. Strube and M. Vidal for their excellent work in the production and processing of the streamer chamber data.

This work was performed at the Fermi National Accelerator Laboratory, which is operated by Universities Research Association, Inc., under contract DE-AC02-76CHO3000 with the U.S. Department of Energy. The work of the University of California, San Diego was supported in part by the National Science Foundation, contract numbers PHY82-05900, PHY85-11584, and PHY88-10221; the University of Illinois at Chicago by NSF contract PHY88-11164; and the University of Washington by NSF contract numbers PHY83-13347 and PHY86-13003. The University of Washington was also supported by the U.S. Department of Energy. The work of Argonne National Laboratory was supported by the Department of Energy, Nuclear Physics Division, under Contract No. W-31-109-ENG-38. The Department of Energy, High Energy Physics Division, supported the work of Harvard University, the University of Maryland, the Massachusetts Institute of Technology under Contract No. DE-AC02-76ER03069, Northwestern University under Contract No. DE-FG02-91ER40684, and Yale University. The Albert-Ludwigs-Universität Freiburg and the University of Wuppertal were supported in part by the Bundesministerium für Forschung und Technologie. The work of the Institute for Nuclear Physics, Krakow, was supported in part by the Polish Committee for Scientific Research.

References

- [1] M. Arneodo et al. (NA9), Phys. Lett. **B145** (1984) 156
- [2] D. Allasia et al. (WA25), Phys. Lett. **B154** (1985) 231
- [3] N.J. Baker et al., Phys. Rev. **D34** (1986) 1251
- [4] M. Arneodo et al. (NA9), Z. Phys. **C34** (1987) 283
- [5] S. Willocq et al. (WA59), Z. Phys. **C53** (1992) 207
- [6] G.T. Jones et al. (WA21), Z. Phys. **C57** (1993) 197
- [7] M.R. Adams et al., Nucl. Inst. and Meth. **A291** (1990) 533
- [8] J.J. Ryan, Ph.D. Thesis, Massachusetts Institute of Technology, 1991
- [9] M.R. Adams et al., Scaled Energy (z) Distributions of Charged Hadrons Observed in Deep-Inelastic Muon Scattering at 490 GeV from Xenon and Deuterium Targets, paper submitted to Phys. Rev. D (1993)
- [10] S. Söldner-Rembold, Ph.D. Thesis, Technische Universität München, 1992
S. Söldner-Rembold, MPI report MPI-PhE/92-17 (1992)
- [11] M.R. Adams et al., Production of charged hadrons by positive muons on deuterium and xenon at 490 GeV, paper submitted to Z. Phys. C (1993)
- [12] G. Ingelman, T. Sjöstrand, LU TP 80-12, University of Lund (1980)
T. Sjöstrand, Comp. Phys. Comm. **27** (1982) 243
- [13] R. Brun et al., GEANT3 Manual, CERN DD/EE/84-1 (1987)
- [14] G. Ingelman, Proceedings of the workshop 'Physics at HERA', Hamburg, Oct. 1991, edited by W. Buchmüller and G. Ingleman, Vol. 3, p. 1366
- [15] T. Sjöstrand, A Manual to the Lund Monte Carlo for Jet Fragmentation and e^+e^- Physics, JETSET version 7.3, June 1991
T. Sjöstrand, Comp. Phys. Commun. **39** (1986) 347; **43** (1987) 367
- [16] E. Eichten et al., Rev. Mod. Phys. **56** (1984) 579; **58** (1986) 1047
- [17] D. Hantke, Ph.D. Thesis, Technische Universität München, 1993
- [18] O.I. Dahl et al., Group A programming note, Lawrence Radiation Lab., p. 126 (1986)
- [19] M.R. Adams et al., Phys. Lett. **B272** (1991) 163
- [20] M.R. Adams et al., Q^2 Dependence of the Average Squared Transverse Energy of Jets in Deep-Inelastic Muon-Nucleon Scattering with Comparison to QCD, paper submitted to Phys. Rev. Lett. (1993)

- [21] M.R. Adams et al., Perturbative QCD Effects Observed in 490 GeV Deep-Inelastic Muon Scattering, paper submitted to Phys. Rev. D (1993)
- [22] M.D. Baker, Ph.D. Thesis, Massachusetts Institute of Technology, 1992
- [23] V.V. Ammosov et al., Phys. Lett. **B93** (1980) 210
- [24] P.K. Malhotra, R. Orava, Z. Phys. **C17** (1983) 85
- [25] W. Bartel et al., Z. Phys. **C20** (1983) 187
- [26] T. Müller, Proc. of the XIVth Int. Symp. on Multiparticle Dynamics, Lake Tahoe (1983), p. 528
- [27] A. Breakstone et al., Phys. Lett. **B135** (1984) 510
- [28] M. Althoff et al., Z. Phys. **C27** (1985) 27
- [29] G.T. Jones et al., Z. Phys. **C27** (1985) 43
- [30] A. Wroblewski, Acta Phys. Pol. **B16** (1985) 379
- [31] M. Derrick et al., Phys. Rev. **D35** (1987) 2639
- [32] W. Geist, Proc. of the Hadronic Session of the 22nd Rencontre de Moriond, Les Arcs (1987), p. 581

meaning of parameter	name of parameter	value of parameter
suppression of diquark-antidiquark pair production in the color field, compared to quark-antiquark production ($P(qq)/P(q)$)	PARJ(1)	0.10
suppression of s quark pair production in the field compared to u or d pair production ($P(s)/P(u)$)	PARJ(2)	0.20
the extra suppression of strange diquark production compared to the normal suppression of strange quarks ($[P(us)/P(ud)]/[P(s)/P(d)]$)	PARJ(3)	0.40
probability that a light meson (containing u and d quarks only) has spin 1, when formed in fragmentation	PARJ(11)	0.50
probability that a strange meson has spin 1	PARJ(12)	0.60

Table 1: Values of some parameters in the Lund JETSET 7.3 program, as used in the present analysis.

a) FS data set

K^0	$\Lambda, \bar{\Lambda}$
$P(\chi^2)_{K^0} > 0.01$ $P(\chi^2)_{K^0} > 0.8 \cdot P(\chi^2)_{\Lambda, \bar{\Lambda}}^*$	$P(\chi^2)_{\Lambda, \bar{\Lambda}} > 0.01$ $P(\chi^2)_{\Lambda, \bar{\Lambda}} > 1.25 \cdot P(\chi^2)_{K^0}^*$
$P(\chi^2)_\gamma < 0.001$	$P(\chi^2)_\gamma < 0.05$
$m(e^+e^-) > 0.05 \text{ GeV}$	$m(e^+e^-) > 0.05 \text{ GeV}$
$\ell > 0.5 \text{ m}$	—
$0.45 \text{ GeV} < m(\pi^+\pi^-) < 0.55 \text{ GeV}$	$\frac{m(p\pi^-)}{m(\bar{p}\pi^+)} < 1.12 \text{ GeV}$

b) SC data set

K^0	$\Lambda, \bar{\Lambda}$
$P(\chi^2)_{K^0} > 0.01$ $P(\chi^2)_{K^0} > 1.25 \cdot P(\chi^2)_{\Lambda, \bar{\Lambda}}^*$	$P(\chi^2)_{\Lambda, \bar{\Lambda}} > 0.01$ $P(\chi^2)_{\Lambda, \bar{\Lambda}} > 0.8 \cdot P(\chi^2)_{K^0}^*$
$P(\chi^2)_\gamma < 0.001$ $P(\chi^2)_{\bar{\Lambda}} < 0.001$	$P(\chi^2)_\gamma < 0.001$ —
$m(e^+e^-) > 0.2 \text{ GeV}$	$m(e^+e^-) > 0.05 \text{ GeV}$
$v < 2 \text{ cm}, v/\ell < 0.1$ $d < 3 \text{ cm}$	$v < 2 \text{ cm}, v/\ell < 0.1$ $d < 3 \text{ cm}, \Theta_{V^0} > 0.1$
$0.46 \text{ GeV} < m(\pi^+\pi^-) < 0.55 \text{ GeV}$	$1.10 \text{ GeV} < \frac{m(p\pi^-)}{m(\bar{p}\pi^+)} < 1.14 \text{ GeV}$

Table 2: Definition of the samples of K^0 , Λ and $\bar{\Lambda}$ candidates: a) FS and b) SC data set. $P(\chi^2)_{V^0}$ is the χ^2 -probability of the kinematic fit for a particular V^0 decay hypothesis. m is the effective mass of the pair of decay particles assuming electron masses (e^+e^-), pion masses ($\pi^+\pi^-$) or proton-pion masses ($p\pi^-$, $\bar{p}\pi^+$) respectively, ℓ is the distance of the decay vertex from the primary interaction vertex, v is the distance by which the V^0 momentum vector (as calculated from the momenta of the decay particles) misses the primary interaction vertex, d is the distance and Θ_{V^0} the angle between the trajectories of the decay particles at the position of the decay vertex. In this table it is assumed that Λ - $\bar{\Lambda}$ ambiguities have already been resolved, and $P(\chi^2)_{\Lambda, \bar{\Lambda}}$ denotes the χ^2 -probability of the kinematic fit of the accepted Λ or $\bar{\Lambda}$ hypothesis.

*) The factors 0.8 and 1.25 were chosen so as to minimize wrong classifications of ambiguous V^0 in the Monte Carlo simulation.

	no. of V^0 candidates in the data	background				total background
		K^0	$\Lambda, \bar{\Lambda}$	γ	other	
a) FS data	1266 K^0	–	5.9%	–	4.5%	10.4%
	123 Λ	6.6%	–	3.8%	6.0%	16.4%
	116 $\bar{\Lambda}$	~ 7%	–	~ 4%	~ 0%	~ 11%
b) SC data	116 K^0	–	1.6%	0.8%	34.6%	37.0%
	58 Λ	1.3%	–	1.3%	28.5%	31.1%

Table 3: Final samples of V^0 candidates in the FS and SC data sets and the amount of background as estimated by Monte Carlo calculations.

sample	% of all events	$\langle W^2 \rangle$ (GeV^2)	$\langle n_{K^0} \rangle$	$\langle n_{\Lambda} \rangle$	$\langle n_{\bar{\Lambda}} \rangle$
A	40.31	315	0.391	0.093	0.029
B	27.00	301	0.435	0.100	0.035
C	32.69	338	0.678	0.101	0.038
A+B+C	100.00	319	0.496	0.097	0.033

Table 4: Relative size and average W^2 of the different Monte Carlo event samples, and average multiplicities of K^0 , Λ and $\bar{\Lambda}$ particles in each of the samples. A – no QCD corrections, B – gluon radiation, C – photon-gluon fusion. The relative statistical error of $\langle n_{K^0} \rangle$ is less than 1%, of $\langle n_{\Lambda} \rangle$ less than 2% and of $\langle n_{\bar{\Lambda}} \rangle$ less than 3%.

x_F interval		K^0	x_F interval		Λ	$\bar{\Lambda}$
-0.3	-0.2	0.097±0.067	-1.0	-0.4	0.033±0.017	
-0.2	-0.1	0.469±0.185	-0.4	-0.2	0.068±0.038	
-0.1	0.0	1.338±0.414	-0.2	0.0	0.079±0.041	
0.0	0.1	1.381±0.139	0.0	0.1	0.094±0.030	0.0869±0.0260
0.1	0.2	0.860±0.072	0.1	0.2	0.054±0.016	0.0663±0.0164
0.2	0.3	0.378±0.039	0.2	0.4	0.026±0.007	0.0325±0.0076
0.3	0.4	0.255±0.034	0.4	0.7	0.0043±0.0024	0.0026±0.0017
0.4	0.6	0.085±0.012				
0.6	1.0	0.006±0.002				

Table 5: Normalized x_F distributions $\frac{1}{N_{ev}} \frac{dN}{dx_F}$ for K^0 , Λ and $\bar{\Lambda}$ particles.

	b
K^0	6.85 ± 0.24
Λ	5.94 ± 1.03
$\bar{\Lambda}$	6.50 ± 0.83

Table 6: Values of the parameter b obtained by fitting the expression $a \exp(-bx_F)$ to the x_F distributions for K^0 , Λ and $\bar{\Lambda}$ in the forward region of the cms.

	total	backward (B)	forward (F)	$\frac{F-B}{F+B}$
K^0	0.52 ± 0.06	0.21 ± 0.06	0.31 ± 0.02	0.19 ± 0.14
Λ	0.078 ± 0.016	0.056 ± 0.016	0.022 ± 0.004	-0.44 ± 0.14
$\bar{\Lambda}$	—	—	0.020 ± 0.003	—

Table 7: Average multiplicities of K^0 , Λ and $\bar{\Lambda}$ particles in the total x_F range, in the backward and forward regions and forward-backward asymmetries, averaged over the W^2 range from 100 to 900 GeV².

	a	b
K^0	-0.14 ± 0.15	0.039 ± 0.013
Λ	-0.03 ± 0.03	0.004 ± 0.003
$\bar{\Lambda}$	-0.08 ± 0.03	0.009 ± 0.002

Table 8: Fitted values of the parameters a and b in the expression $a + b \cdot \ln(W^2/\text{GeV}^2)$ for the average forward multiplicities of K^0 , Λ and $\bar{\Lambda}$ particles in the W^2 range from 100 to 900 GeV².

x_F interval	a	b
0.0–0.1	-0.060 ± 0.201	0.017 ± 0.016
0.1–0.3	-0.058 ± 0.092	0.015 ± 0.008
0.3–1.0	0.047 ± 0.042	-0.001 ± 0.004

Table 9: Fitted values of the parameters a and b in the expression $a + b \cdot \ln(W^2/\text{GeV}^2)$ for the average multiplicity of K^0 mesons in three x_F bins.

W^2 range (GeV ²)	$x_F > 0$	$0 < x_F < 0.1$	$0.1 < x_F < 0.3$	$x_F > 0.3$	all x_F
100 – 200	0.244±0.029	0.086±0.052	0.110±0.020	0.042±0.007	0.423±0.084
200 – 300	0.263±0.028	0.161±0.061	0.100±0.014	0.038±0.007	0.537±0.112
300 – 400	0.342±0.037	0.140±0.034	0.123±0.017	0.043±0.010	0.443±0.122
400 – 500	0.402±0.049	0.173±0.044	0.142±0.023	0.067±0.018	0.581±0.172
500 – 600	0.391±0.049	0.188±0.041	0.142±0.024	0.043±0.017	0.831±0.179
600 – 900	0.320±0.038	0.155±0.026	0.143±0.027	0.032±0.012	0.545±0.281

Table 10: Average multiplicity of K^0 mesons as a function of W^2 , for different regions of x_F . The values in the individual x_F bins do not add up exactly to the values for the whole forward region, because the experimental data in the various x_F regions were corrected separately and independently.

W^2 range (GeV ²)	$\Lambda, x_F > 0$	$\bar{\Lambda}, x_F > 0$
100 – 200	0.0145±0.0050	0.0077±0.0034
200 – 300	0.0175±0.0067	0.0192±0.0064
300 – 400	0.0149±0.0080	0.0309±0.0098
400 – 900	0.0280±0.0065	0.0314±0.0065

Table 11: Average forward multiplicity of Λ and $\bar{\Lambda}$ hyperons as a function of W^2 .

β (GeV ⁻²)	backward	forward	p_T^2 range used in fit (GeV ²)
K^0	3.21 ± 1.22	3.12 ± 0.19	0-2.0
$0.0 < x_F < 0.1$		3.80 ± 0.43	0-2.0
K^0 $0.1 < x_F < 0.3$		3.12 ± 0.32	0-2.0
$0.3 < x_F$		1.92 ± 0.28	0-2.0
Λ	3.30 ± 0.87	2.72 ± 0.64	0-1.4
$\bar{\Lambda}$	—	2.58 ± 0.44	0-1.4

Table 12: Values of the slope parameter β obtained by fitting the expression $\alpha \exp(-\beta p_T^2)$ to the p_T^2 distributions for K^0 , Λ and $\bar{\Lambda}$ in the backward and forward region of the cms.

Figure Captions

- Fig. 1 Distribution of the effective ($\pi^+\pi^-$) and ($p\pi^-$) mass in the final samples (however, before applying the effective mass cuts) of K^0 and Λ candidates respectively, in the FS data set. The solid line in the K^0 plot is the result of fitting the sum of a constant and two Gaussian functions to the distribution in the mass range $0.45 \text{ GeV} < m(\pi^+\pi^-) < 0.55 \text{ GeV}$. The solid line in the Λ plot shows the Gaussian function obtained by fitting the Λ data in the mass range $1.105 \text{ GeV} < m(p\pi^-) < 1.125 \text{ GeV}$.
- Fig. 2 Normalized x_F distributions $\frac{1}{N_{ev}} \frac{dN}{dx_F}$ for K^0 , Λ and $\bar{\Lambda}$ particles. The predictions of the Lund model are drawn as dashed (no QCD) and solid (with QCD) lines.
- Fig. 3 Average forward multiplicity as a function of x_{Bj} , Q^2 and W^2 for K^0 , Λ and $\bar{\Lambda}$ particles. The predictions of the Lund model are drawn as dashed (no QCD) and solid (with QCD) lines. The results of straight-line fits to the data points are represented by dotted lines.
- Fig. 4 Average multiplicity of K^0 mesons as a function of W^2 , for three bins of x_F in the forward region. The predictions of the Lund model are drawn as dashed (no QCD) and solid (with QCD) lines. The results of straight-line fits to the data points are represented by dotted lines.
- Fig. 5 Average forward multiplicity of K^0 mesons from this experiment (E665) and from νp and $\bar{\nu} p$ scattering [6] as a function of W^2 .
- Fig. 6 Average total multiplicity of K^0 mesons as a function of W^2 , from this experiment (E665), from a μp [4] and from several (anti-)neutrino-nucleon experiments [3, 5, 6].
- Fig. 7 Average total multiplicity of Λ hyperons as a function of W^2 , from this experiment (E665), from a μp [4] and from several (anti-)neutrino-nucleon experiments [3, 5, 6].
- Fig. 8 Normalized p_T^2 distributions $\frac{1}{N_{ev}} \frac{dN}{dp_T^2}$ for K^0 mesons, in three bins of x_F in the forward region. The predictions of the Lund model are drawn as dashed (no QCD) and solid (with QCD) lines. The results of straight-line fits to the data points are represented by dotted lines.
- Fig. 9 Average p_T^2 as a function of x_F for K^0 , Λ and $\bar{\Lambda}$ particles. The lines represent the predictions of the Lund model from different Monte Carlo event samples: A (no QCD, dashed lines), A+B (no QCD + gluon emission, dashed-dotted lines), A+C (no QCD + photon-gluon fusion, dotted lines) and A+B+C (solid lines).
- Fig. 10 Average p_T^2 as a function of W^2 for the forward and the backward region, for K^0 , Λ and $\bar{\Lambda}$ particles. The predictions of the Lund model are drawn as dashed (no QCD) and solid (with QCD) lines.

- Fig. 11 Average p_T^2 of K^0 mesons as a function of W^2 , for three bins of x_F in the forward region. The predictions of the Lund model are drawn as dashed (no QCD) and solid (with QCD) lines.
- Fig. 12 Average p_T^2 of K^0 mesons as a function of Q^2 , for three bins of x_F in the forward region. The predictions of the Lund model are drawn as dashed (no QCD) and solid (with QCD) lines.
- Fig. 13 K^0/π ratios as a function of x_F and, for the forward region, as a function of W^2 . The predictions of the Lund model (including QCD corrections) are drawn as solid ($s/u = 0.20$) and dashed-dotted ($s/u = 0.30$) lines.
- Fig. 14 Average forward multiplicity of K^0 mesons as a function of W^2 . The predictions of the Lund model (including QCD corrections) are drawn as solid ($s/u = 0.20$) and dashed-dotted ($s/u = 0.30$) lines.
- Fig. 15 Ratio $\langle n_\Lambda \rangle / \langle n_{\bar{\Lambda}} \rangle$ of average Λ and $\bar{\Lambda}$ multiplicities as a function of x_F , p_T^2 and W^2 in the forward region. The predictions of the Lund model are drawn as dashed (no QCD) and solid (with QCD) lines.

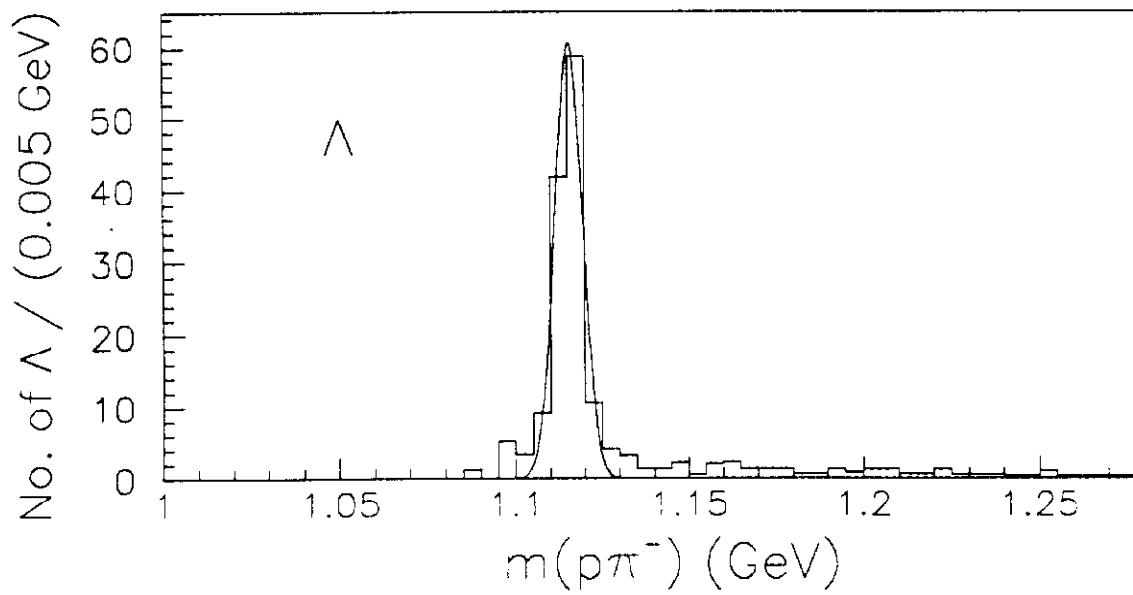
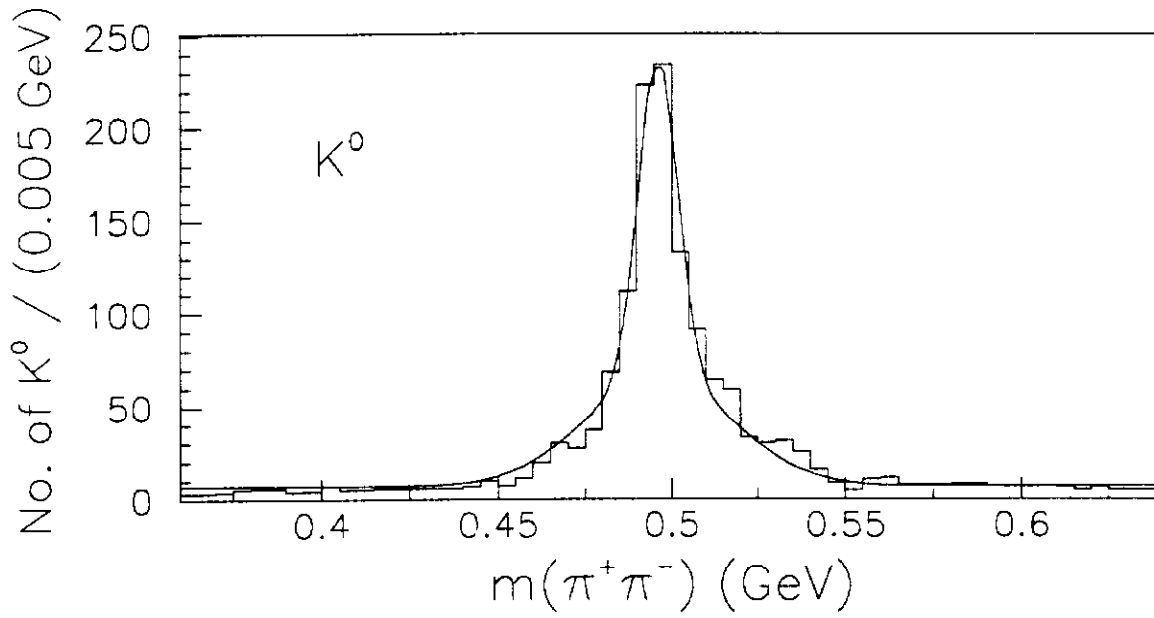


Fig. 1

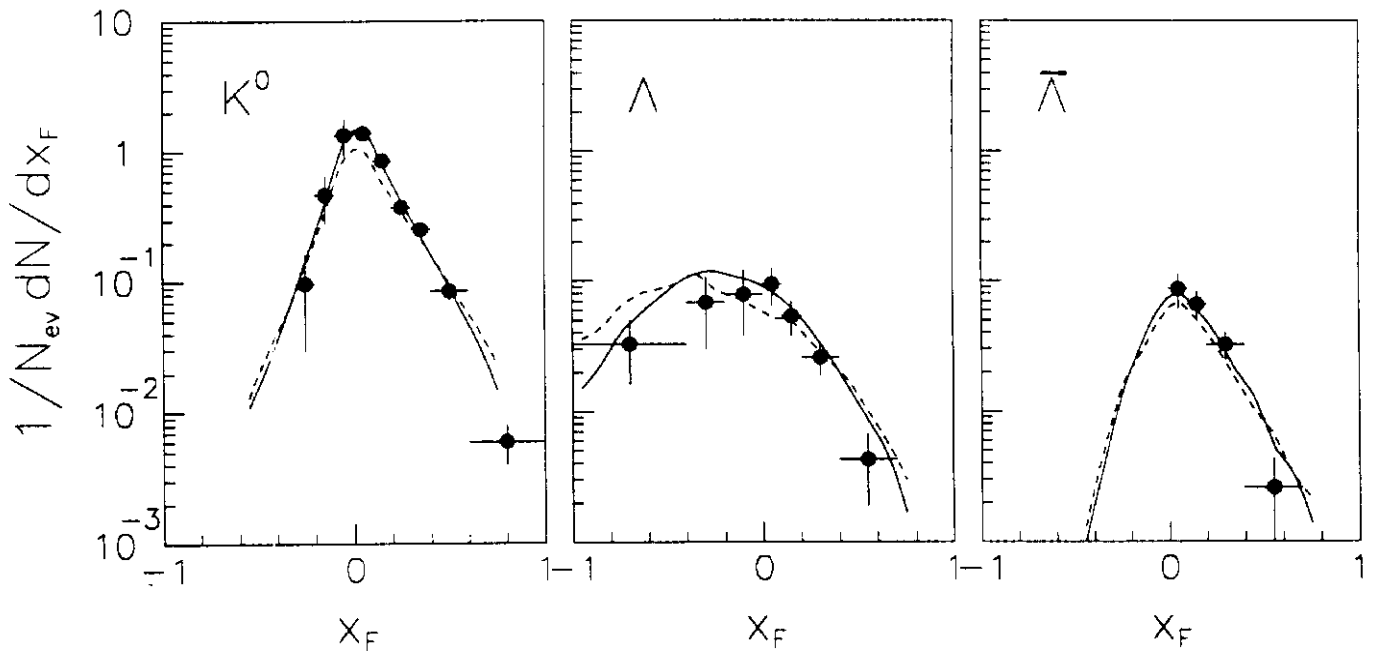


Fig. 2

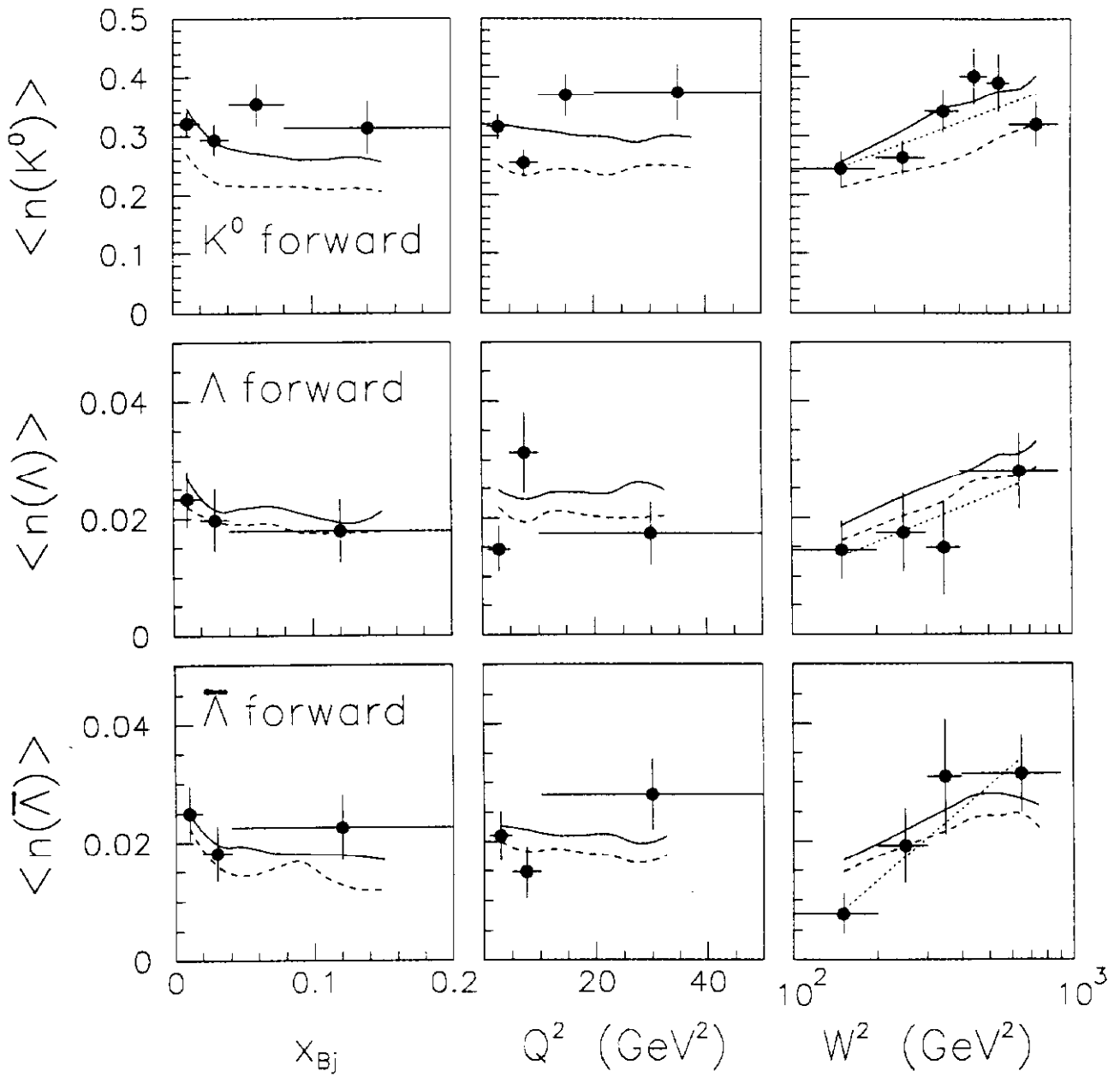


Fig. 3

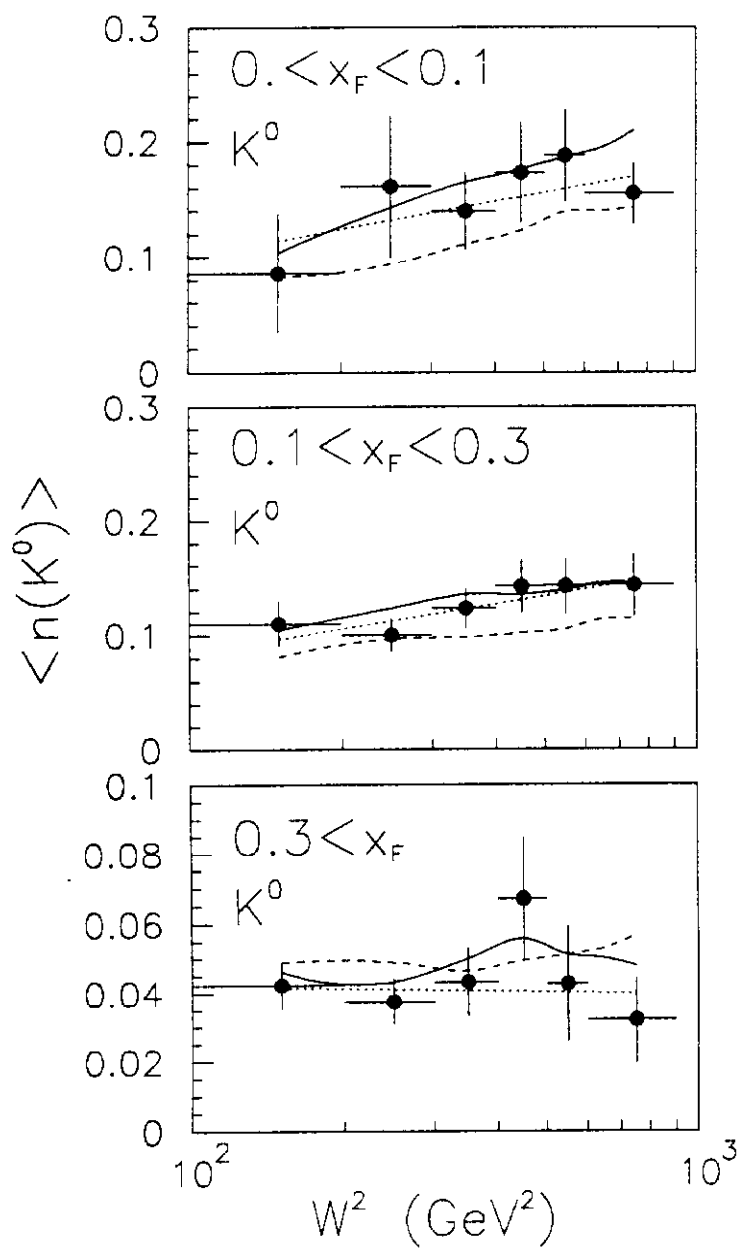


Fig. 4

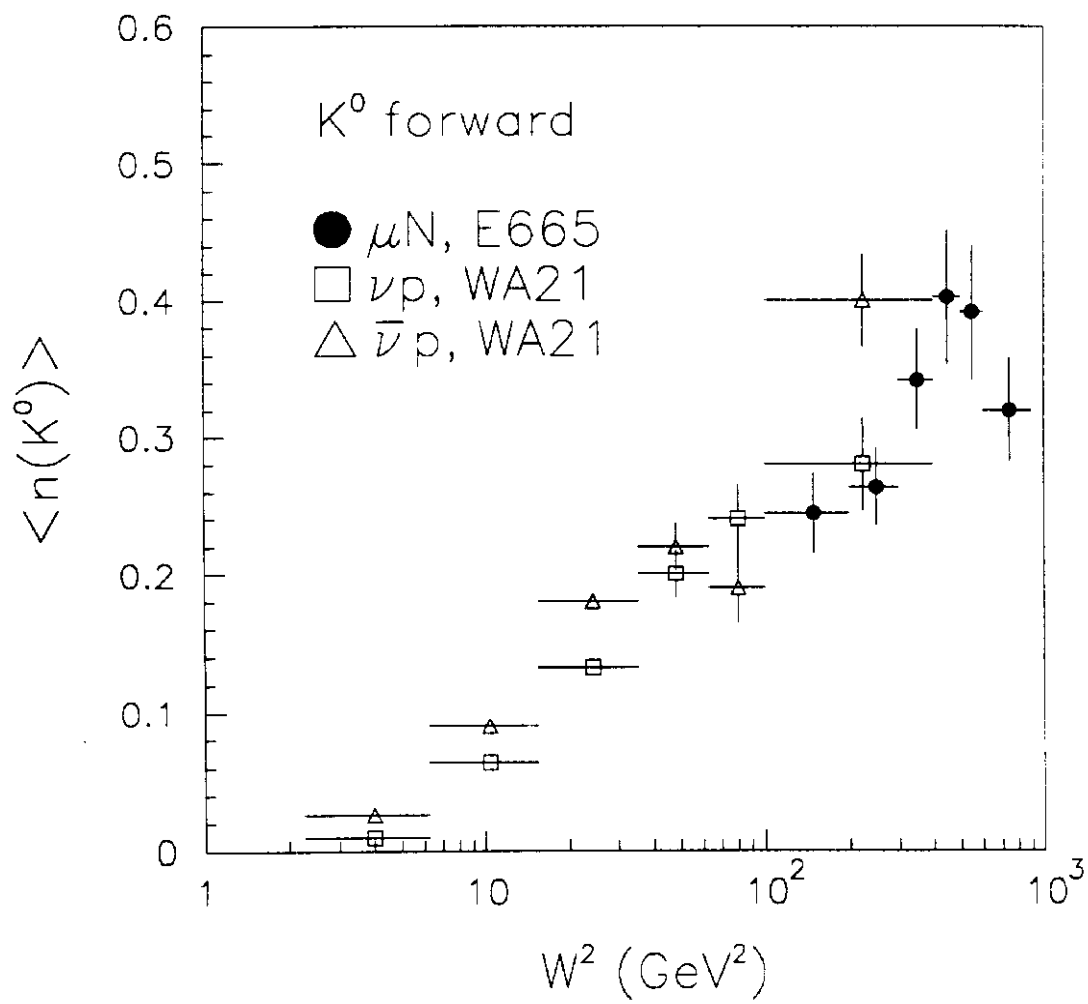


Fig. 5

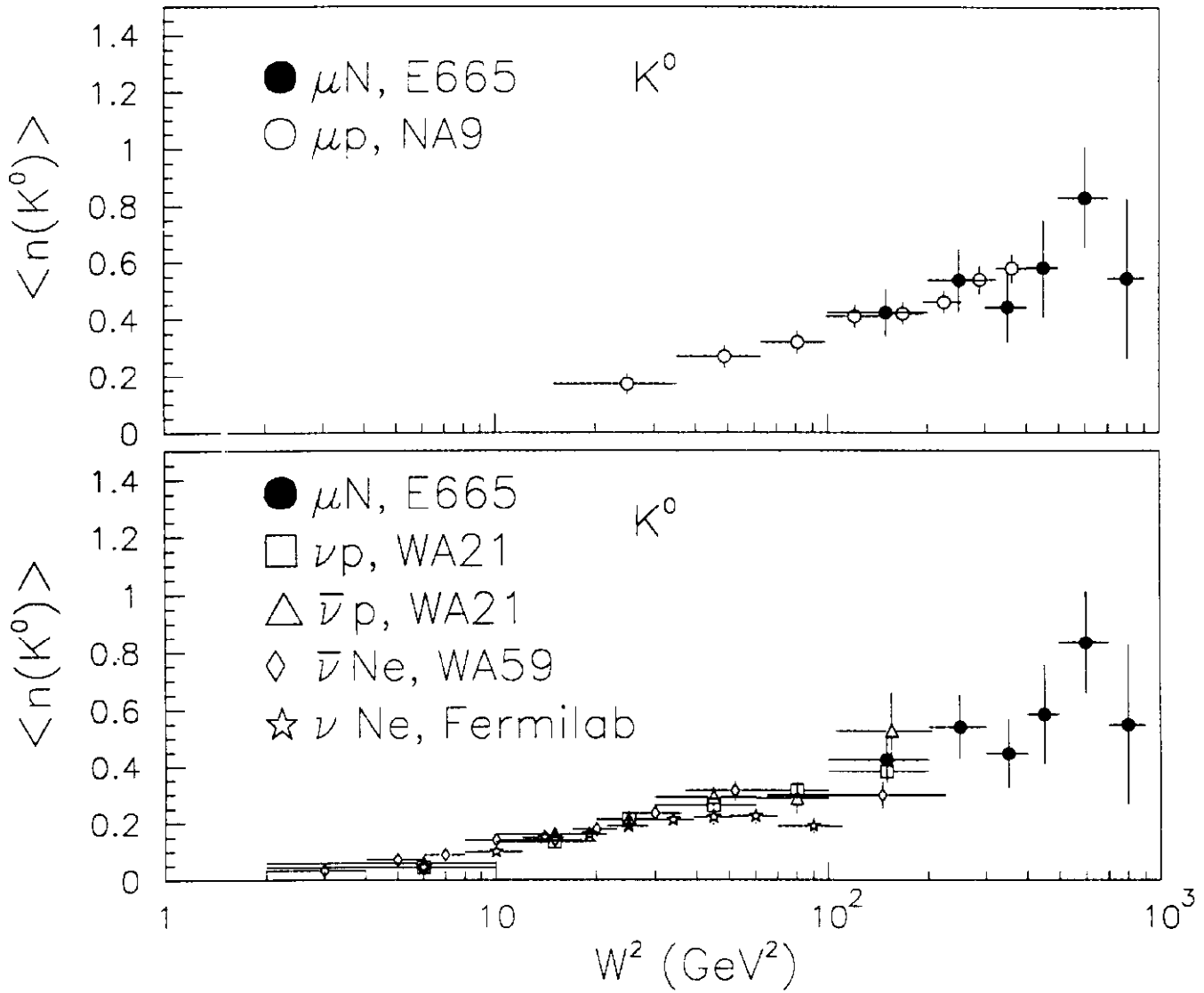


Fig. 6

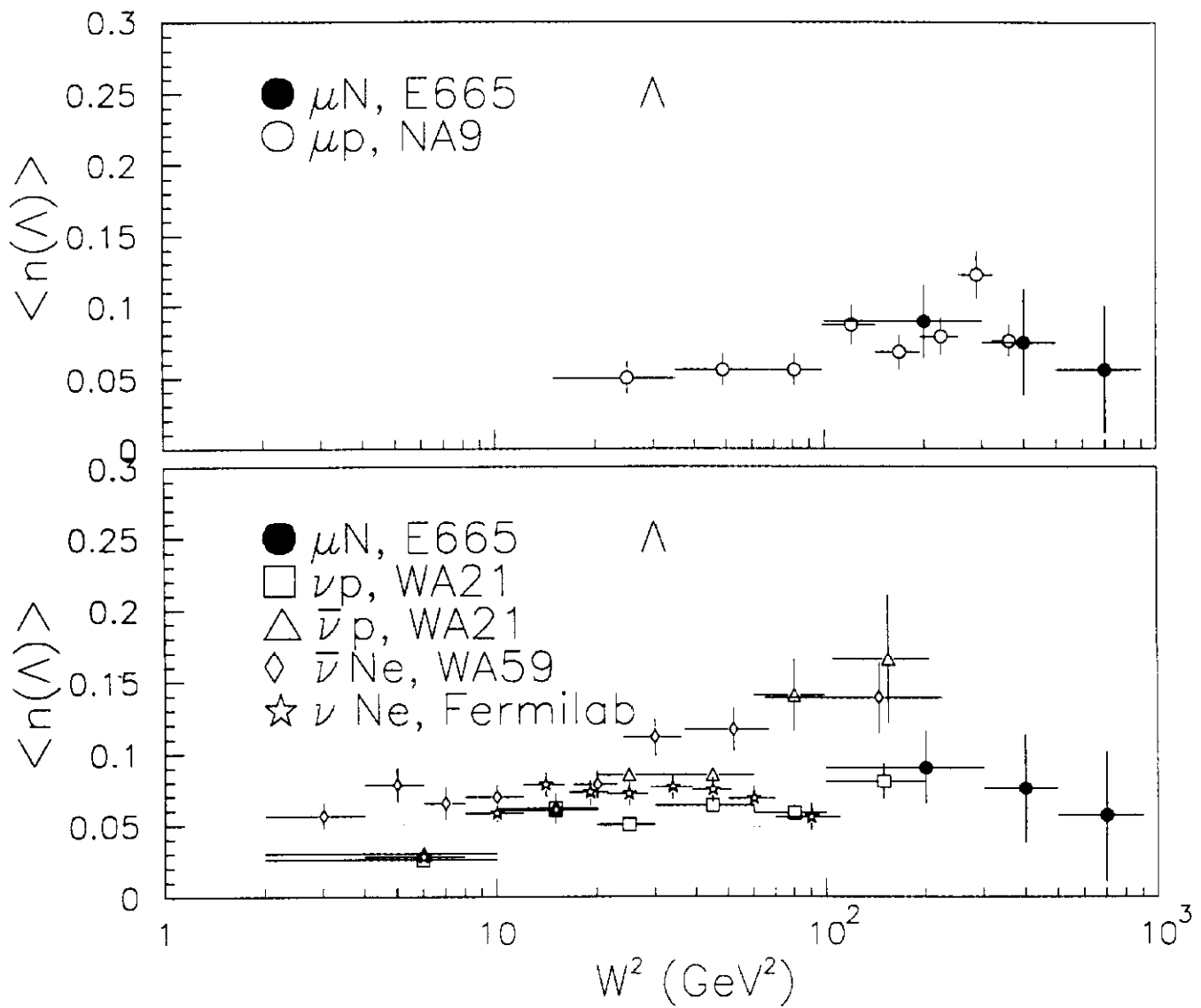


Fig. 7

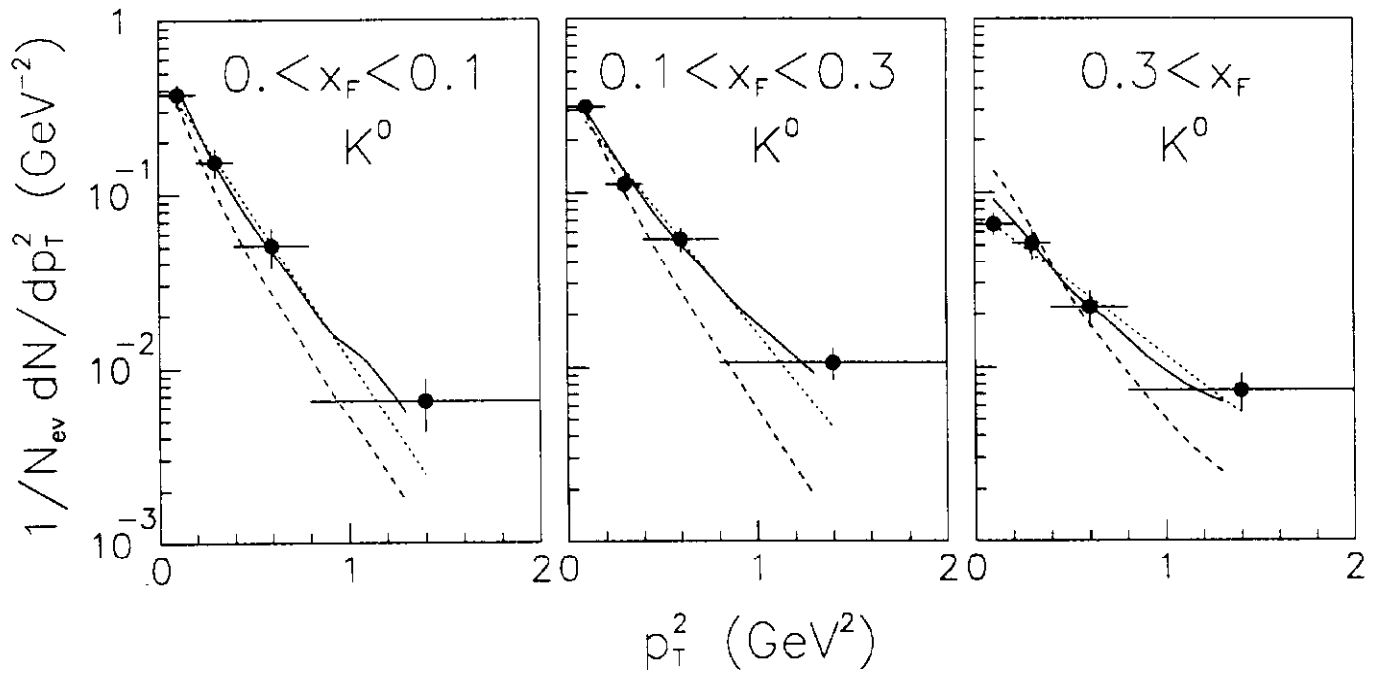


Fig. 8

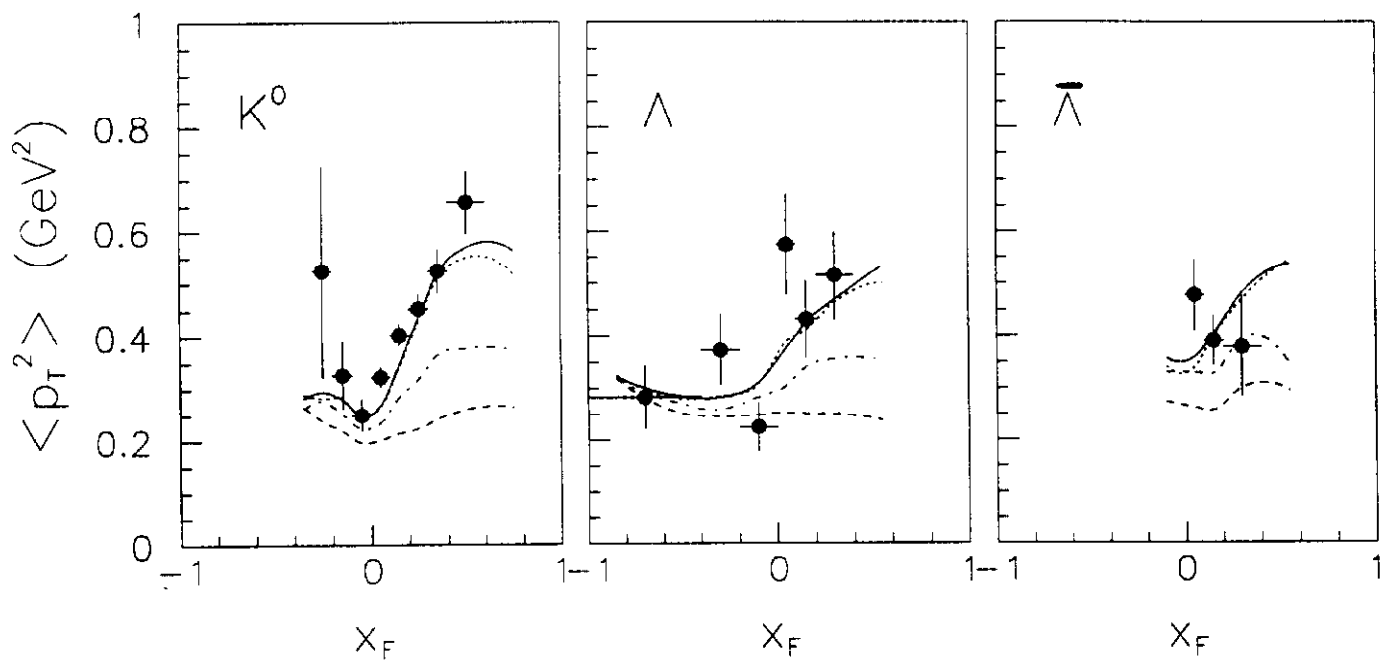


Fig. 9

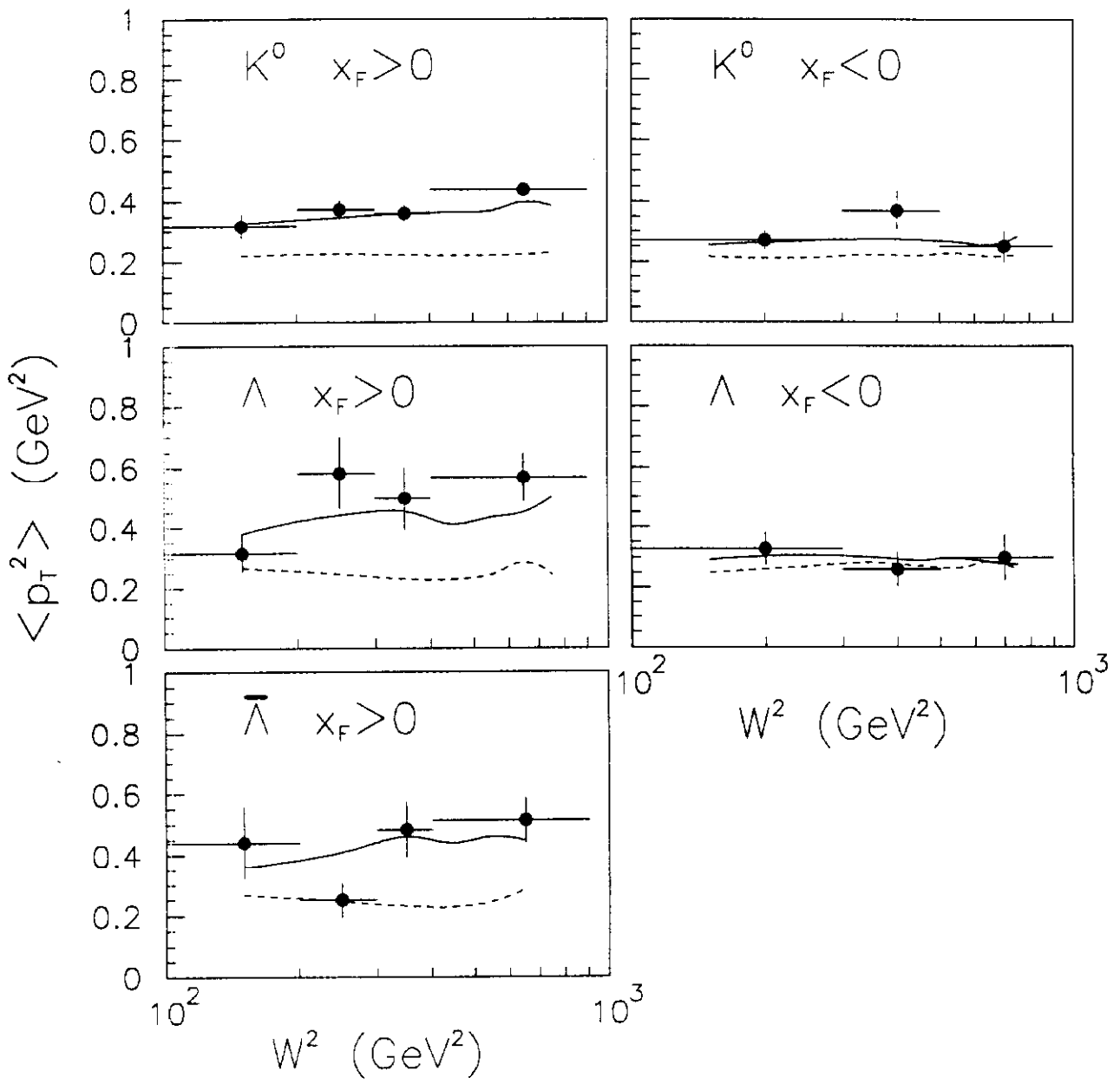


Fig. 10

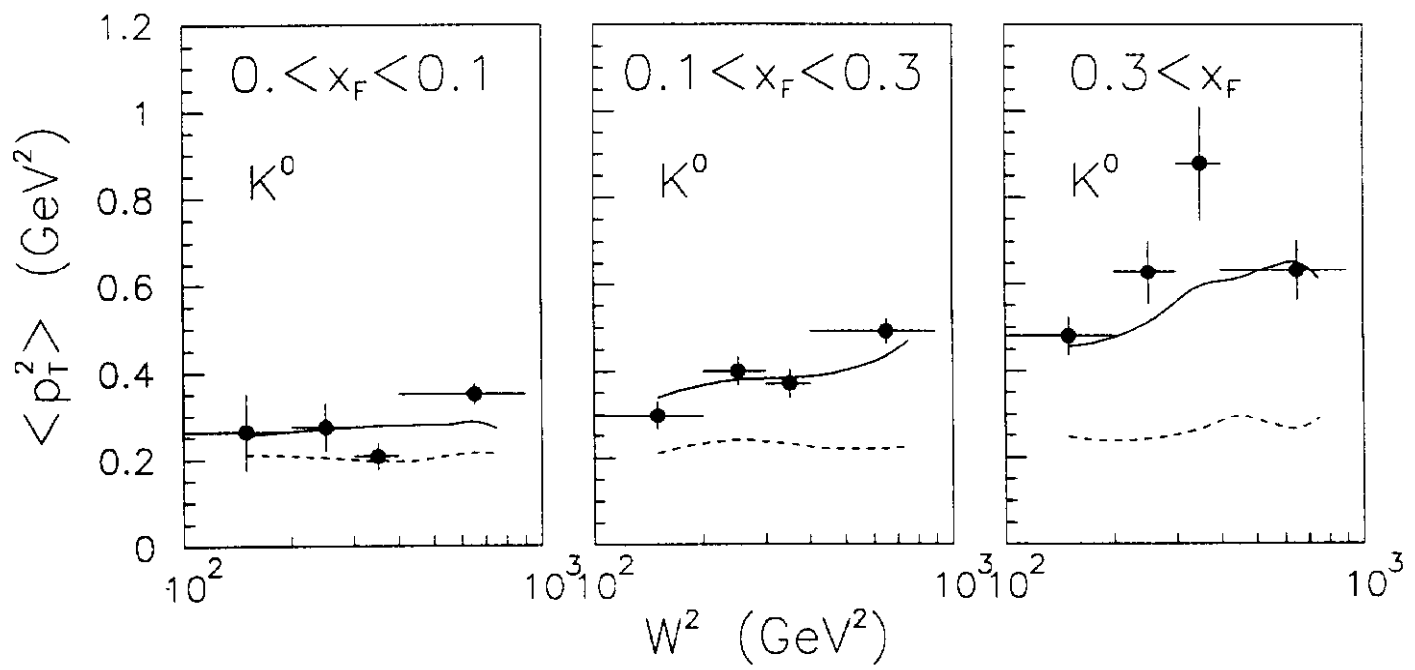


Fig. 11

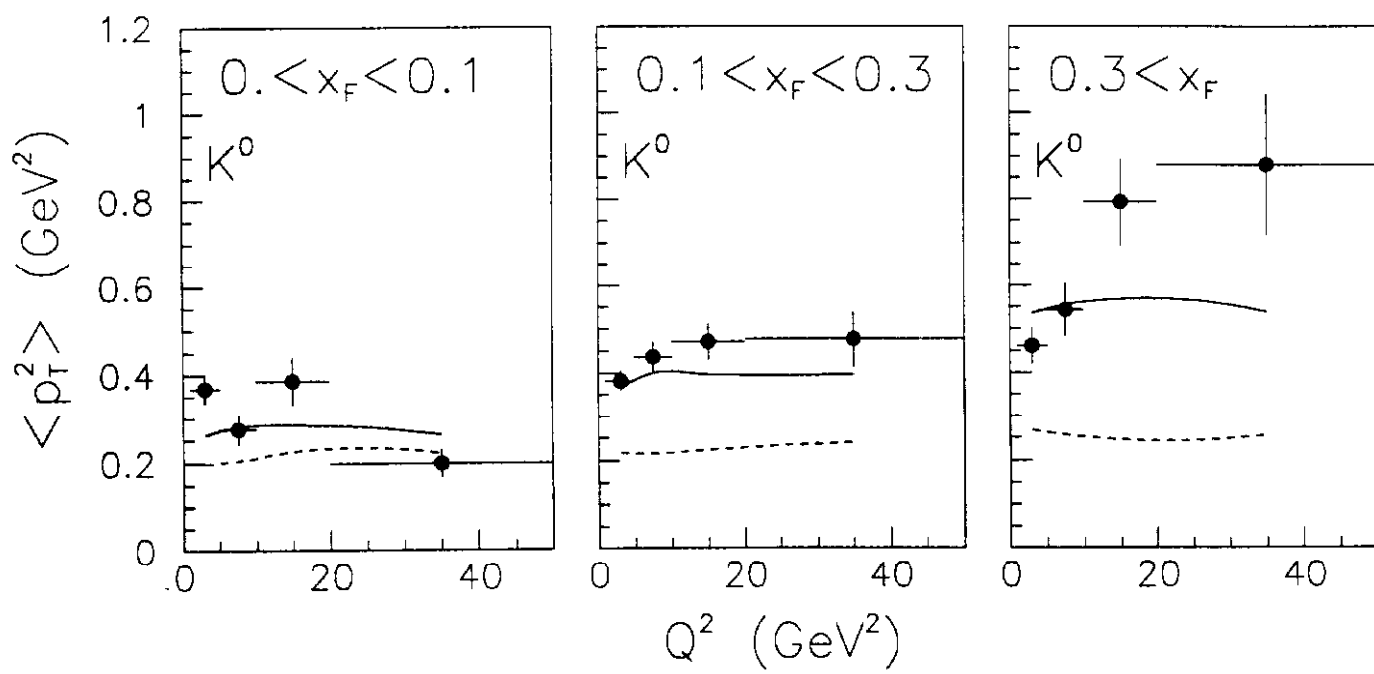


Fig. 12

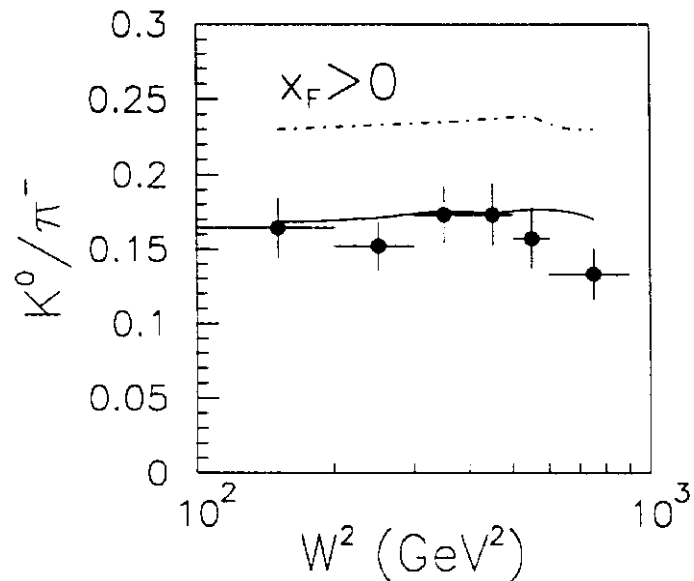
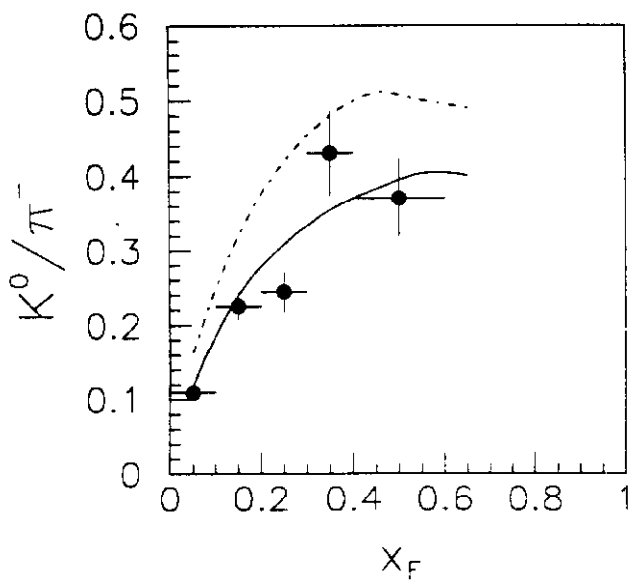
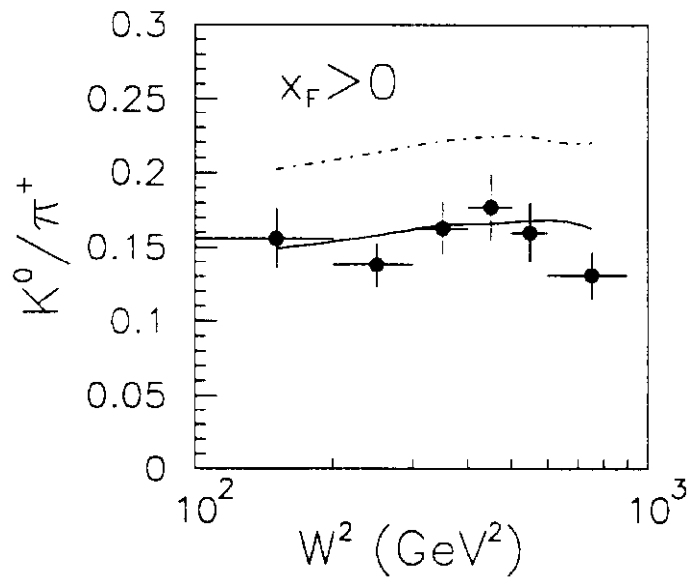
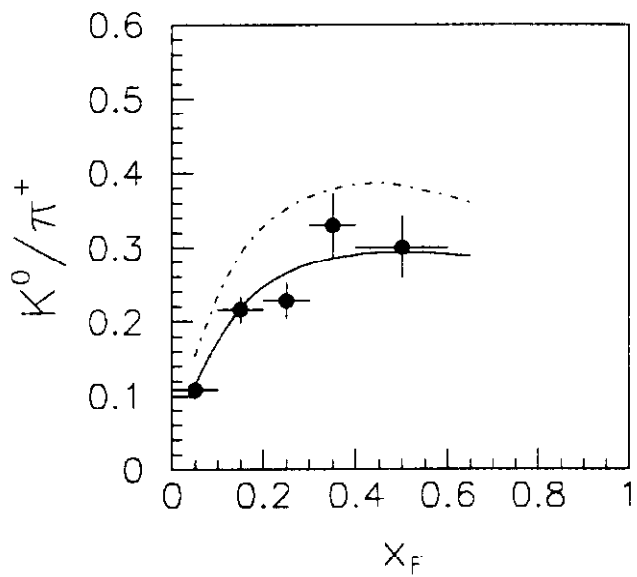


Fig. 13

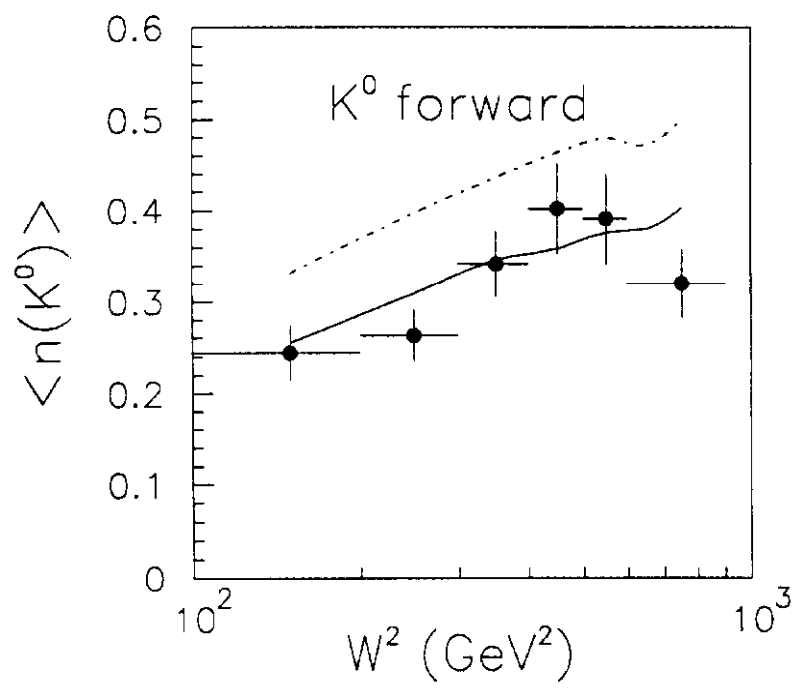


Fig. 14

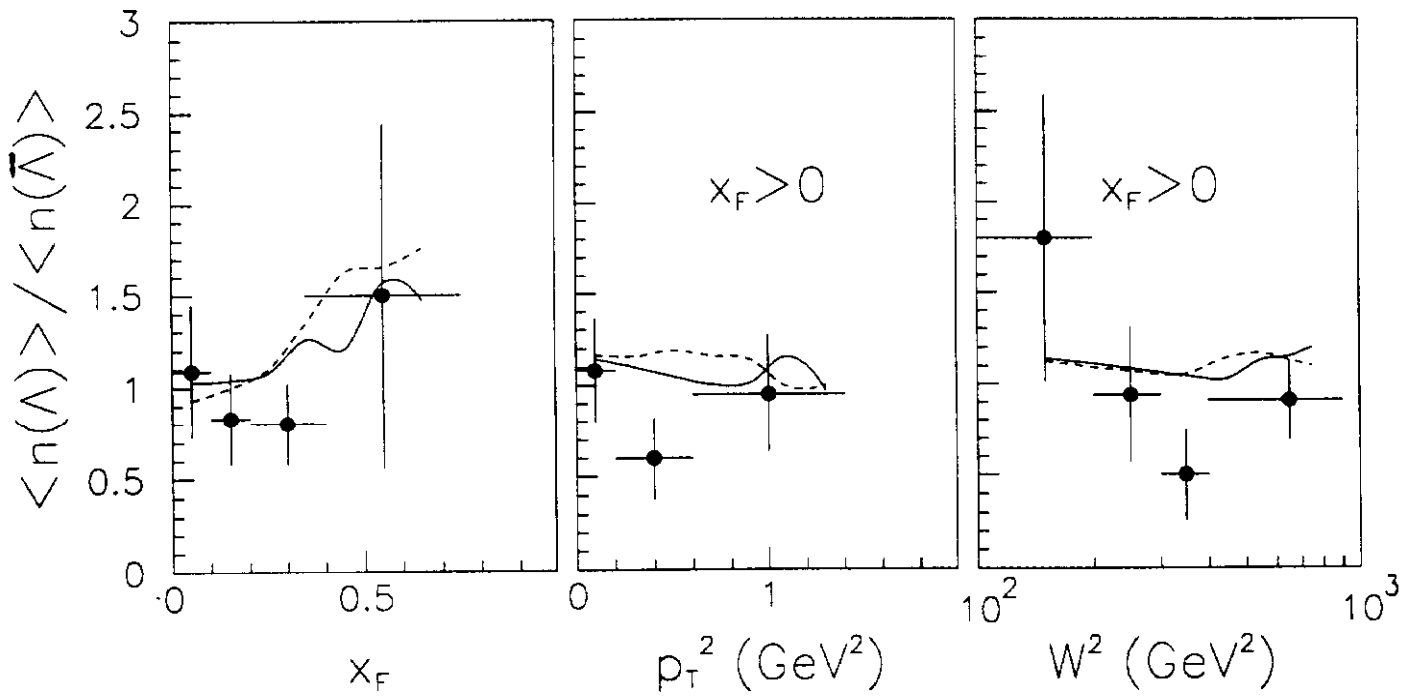


Fig. 15